Journal of Asian Earth Sciences 156 (2018) 189–200

Contents lists available at ScienceDirect

Journal of Asian Earth Sciences

journal homepage: www.elsevier.com/locate/jseaes

Full length article

Changes in detrital input, ventilation and productivity in the central Okhotsk Sea during the marine isotope stage 5e, penultimate interglacial period

Francisco J. Jimenez-Espejo[a,*], Antonio García-Alix[b], Naomi Harada[c], André Bahr[d,e], Saburo Sakai[a], Koichi Iijima[f], Qing Chang[g], Keiko Sato[f,h], Katsuhiko Suzuki[f], Naohiko Ohkouchi[a]

[a] Department of Biogeochemistry, JAMSTEC, Yokosuka, Japan
[b] Departamento de Estratigrafía y Paleontología, University of Granada, Spain
[c] Research and Development Center for Global Change, JAMSTEC, Yokosuka, Japan
[d] Institute of Geosciences, University Frankfurt, Frankfurt, Germany
[e] Institute of Earth Sciences, Heidelberg University, Heidelberg, Germany
[f] Research and Development Center for Submarine Resources, JAMSTEC, Yokosuka, Japan
[g] Department of Solid Earth Geochemistry, JAMSTEC, Yokosuka, Japan
[h] Department of Chemistry and Biochemistry, National Institute of Technology, Fukushima College, Iwaki, Japan

ABSTRACT

By presenting benthic foraminifera isotope profiles and bulk geochemical composition of core sediments, we offer a mutiproxy reconstruction of the central Okhotsk Sea oceanography between ~130 to and ~115 kyr, related to the marine isotopic stage 5e (MIS 5e). Sediments from the site MR0604-PC7A have been compared with paleo- sea surface temperatures and other records. This multiparameter approach allowed to recognize three periods for MIS 5e evolution, characterized by variations in marine productivity and bottom oxygenation. These variations have been ultimately associated with the production of Okhotsk Sea Intermediate Water and the presence or absence of nutrient contribution from the Pacific Deep Water into central Okhotsk Sea. Aeolian input reconstructed by Th/Sc ratio indicates higher values during the MIS 6 and MIS 5d compared with the MIS 5e. Eu* values indicate an input of detrital material from Kurile Islands and East-Kamchatka during the late MIS 5e, absent during the early MIS 5e and glacial periods.

1. Introduction

The Arctic and Subarctic Northern Hemisphere realm is considered to be the region on Earth for which major environmental changes are expected (Screen and Simmonds, 2010). Assessing environmental constrains associated with a climate warming is important for predictive modelling. One of the best ways to make realistic models is using high-resolution studies of the penultimate interglacial period (Otto-Bliesner et al., 2006; Hoffman et al., 2017). Although this period is not a perfect equivalent to the Holocene because of different orbital parameters (Loutre and Berger, 2003; Capron et al., 2017), nor a straight analogy for future greenhouse global warming, the study of this most recent warm scenario (the Marine Isotope Stage 5e –(MIS 5e)) provides a natural record of potential environmental changes related to a predicted global temperature increase. In this way, during the MIS 5e the last major sea level rise took place, linked to important ice volume changes and oceanographic reorganization (Thomas et al., 2009). Therefore, the study of this time interval is a *key point* in order to know the real environmental responses associated with warming scenarios.

Aiming to understand the detailed changes that lead to glacial/interglacial transitions in subarctic regions and their corresponding climate and environmental responses, we selected the Okhotsk Sea area in the northwestern Pacific (Fig. 1). The high productivity and the intense intermediate water formation make the studied region one of the worlds important CO_2 sinks (e.g., Tsunogai et al., 1992; Takahashi, 1998; Takahashi et al., 2000; Otsuki et al., 2003). For this reason our study will have a special focus in water column variations. In addition, this area is the southernmost marginal sea in the world covered by sea ice at present in the Northern Hemisphere, being one of the less studied subarctic regions and one of the most sensitive to climate changes (e.g.,

* Corresponding author.
E-mail addresses: fjjspejo@jamstec.go.jp (F.J. Jimenez-Espejo), agalix@ugr.es (A. García-Alix), haradan@jamstec.go.jp (N. Harada), andre.bahr@geow.uni-heidelberg.de (A. Bahr), saburos@jamstec.go.jp (S. Sakai), kiijima@jamstec.go.jp (K. Iijima), qchang@jamstec.go.jp (Q. Chang), keisato@fukushima-nct.ac.jp (K. Sato), katz@jamstec.go.jp (K. Suzuki), nohkouchi@jamstec.go.jp (N. Ohkouchi).

https://doi.org/10.1016/j.jseaes.2018.01.032
Received 24 July 2017; Received in revised form 15 January 2018; Accepted 28 January 2018
Available online 31 January 2018
1367-9120/

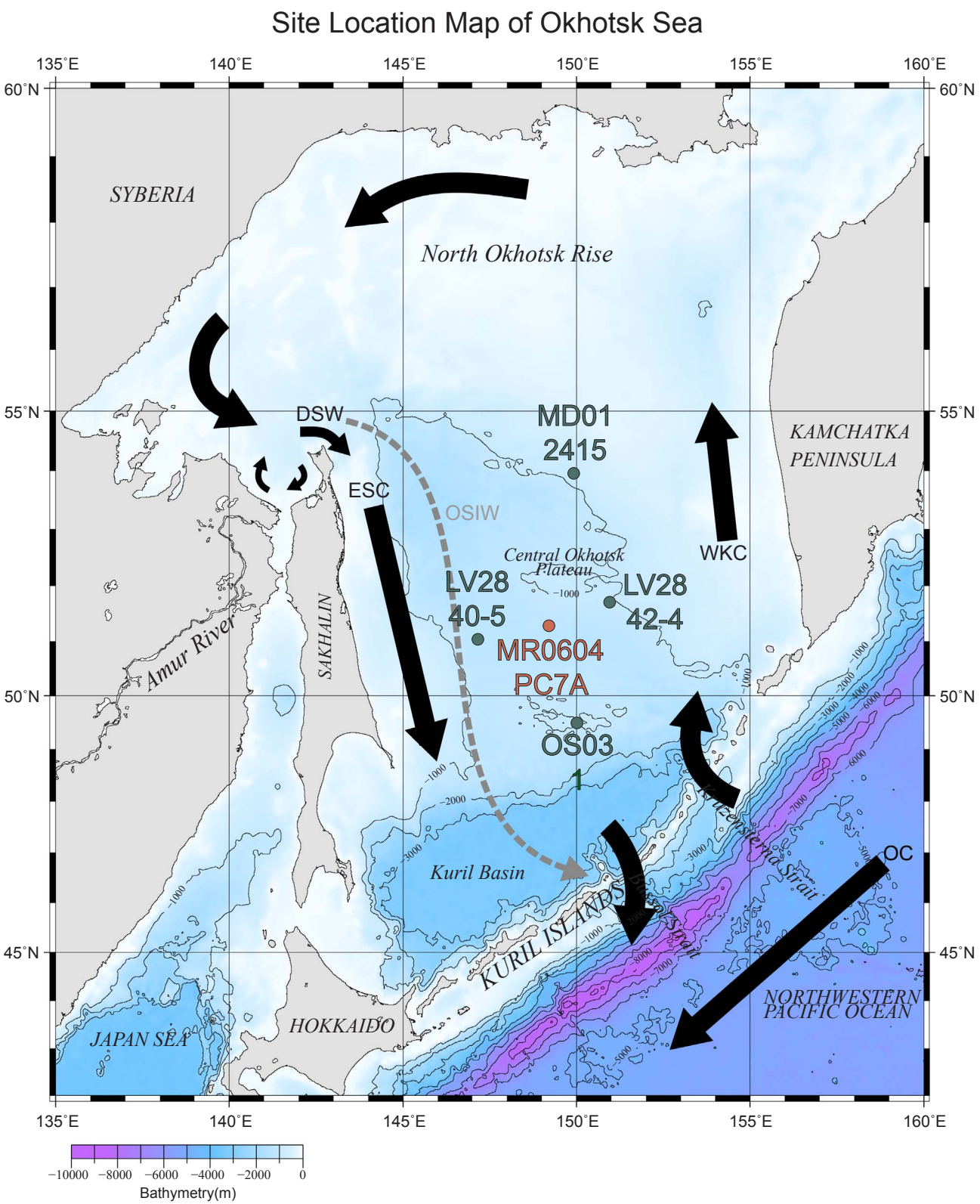

Fig. 1. Okhotsk Sea bathymetry map and location of core PC7A. The map was produced by Japan Oceanographic Data Center. Black arrows represent surface circulation: OC = Oyashio Current, WKC = West Kamchatka Current, ESC = East Sakhalin Current, WSAW = Western Subarctic Water. Dotted line indicates the path of the Dense Shelf Water (DSW) and Okhotsk Sea Intermediate Water (OSIW).

Hays and Morley, 2004).

The special character of the Okhotsk Sea and their relatively high sedimentation rates make this region a key location to obtain records for climate-related responses at centennial/millennial scale (e.g., Gorbarenko et al., 2012; Chebykin et al., 2015). Paleoceanographic studies in the Okhotsk Sea were scarce in 20th century mainly due to the inaccessibility for foreign scientist (Gorbarenko et al., 1998). However, in spite of the increasing number of studies along this century

(e.g., Nürnberg and Tiedemann, 2004; Sakamoto et al., 2006; Liu et al., 2006, Okazaki et al., 2010; 2014; Wang et al., 2017), the detailed mechanisms of the transition from glacial to interglacial and back to glacial conditions in this area remain poorly understood (e.g., Levitan and Lavrushin, 2009). The studies dedicate to the MIS 5 (e.g., Sato et al., 2002; Iwasaki et al., 2012; Khim et al., 2012; Gorbarenko et al., 2017) are mainly focussed on marine productivity mechanisms during glacial/interglacial periods and links with East Asian monsoon dynamics but a detailed study along the MIS 5e multiproxy discussion of detrital sources and productivity modes is not achieved. Reconstructing the water exchange between the Okhotsk Sea and the North Pacific is especially important because it constitutes a key component of the global ocean thermohaline circulation (e.g., Hong et al., 2009).

In this paper, we present a high-resolution study comparing directly atmospheric input, deep-water oxygenation and marine productivity among other records from the Okhotsk Sea between ~130 kyr to and ~115 kyr. Our new record provides further insight into the paleoclimatic variability, paleoenvironment responses and paleohydrologic changes for the penultimate glacial/interglacial transition from a region still poorly understood and underrepresented in the global paleoceanographic database.

2. Modern hydrography, marine productivity and climate conditions in the Okhotsk Sea

The Okhotsk Sea is a marginal sea located in the northwestern sector of the Pacific Ocean, surrounded by the mainland of Kamchatka Peninsula, and Far East Russia (Okhotsk volcanic Belt), and by the Sakhalin, Hokkaido, and Kurile Islands. It is connected to the Pacific Ocean by some straits between the Kurile Islands, and to the Japan Sea in the west and southwest by the Tatarsky and Soya straits (Fig. 1).

Sea-ice formation in the Okhotsk Sea depends on the variability in intensity and position of the Siberian High and Aleutian Low, which is related to winter East Asian monsoon oscillations (Wallace, 2000). In spite of its mid-latitude location, the climatic conditions are comparable to those of a polar ocean. In this sense, the area is characterized by the largest seasonal sea-ice coverage in the middle-latitudes of the northern hemisphere. It is covered by sea-ice about two-thirds during the winter (Itoh and Ohshima, 2000), and usually free of ice from June/July to October (Parkinson, 2000). This sea-ice is mostly formed in the northwestern region, and posteriorly it expanded to most of the Okhotsk Sea due to the effect of winter winds and the East Sakhalin Current (Kimura and Wakatsuchi, 1999; Simizu et al., 2014). Detrital sediments are incorporated within this ice near mainland, and subsequently released into the open sea by drifting sea-ice after the spring melt (Sakamoto et al., 2006).

Besides of a regional impact, the Okhotsk Sea influences the climate and the ocean oscillations at global scales (e.g., Hong et al., 2009), boosting the generation of the North Pacific Intermediate Water (controlled by sea surface salinity and sea surface temperature (SST)). This is caused by the large development of sea-ice in this basin and the development of local intermediate waters saturated in oxygen in the northwestern shelf (cold, denser and saline), which flow into the Pacific Ocean (Talley, 1991; Wong et al., 1998). This cold SST directly influences the development of the atmospheric high-pressure system in the southwestern Okhotsk Sea, making the Okhotsk Sea a driving force for the regional atmospheric circulation as well.

The surface circulation in the Okhotsk Sea is a cyclonic gyre. Most present water is originated from the Pacific Ocean and enters the Okhotsk Sea via two gateways at Kurile Islands; water exchange with the Japan Sea is less important (Itoh et al., 2003). The characteristic property of the hydrology of the Okhotsk Sea is the development of the so-called dichothermal cold waters at depths of 50–150 m with temperatures < 0 °C, which are formed during the winter cooling of surface water (ice formation) and remain through the whole year. During autumn and winter, on the northern and western shelves, extensive brine rejection caused by sea ice formation leads to the formation of the oxygenated of Okhotsk Sea Intermediate Water (OSIW) in depths of 200–1000 m (Wong et al., 1998). Below the OSIW has been described the Pacific Deep Water (PDW) intruding the Okhotsk Sea mainly via Krusenstherna Strait. These Pacific waters are CO_2 enriched and very old. The Okhotsk Sea, together with the northwestern part of the Pacific Ocean and the Bering Sea represent the final section of the global salinity conveyor belt (Broecker, 1991). In this area of the northwestern Pacific Ocean, water masses are the oldest waters of the World Ocean and have the highest content in nutrients. This circumstance explains such high primary productivity of these areas.

The biological production is mainly dominated by siliceous microplankton in the Okhotsk Sea; however, a succession of blooms of dominant phytoplankton species (first calcitic and subsequently siliceous) can be found seasonally from spring to autumn (Boerse et al., 2000; Nimmergut and Abelman, 2002). Primary production is boosted by the nutrient supply, seasonal solar insolation and the ice melting (Saitoh et al., 1996; Sorokin and Sorokin, 1999; Seki et al., 2004; Okazaki et al., 2005; Okunishi et al., 2007), with Fe as limiting nutrient (Suzuki et al., 2014). The organic matter oxidation consumes oxygen creating an oxygen minimum zone between 750 and 1500 m (Salyuk et al., 2003).

There is an important contribution of fresh water and terrestrial material to the Sea of Okhotsk from the Amur River, one of the largest rivers in the world, flowing into the western sector of the Okhotsk Sea (Ogi and Tachibana, 2006). However, most of the detrital input by the Amur does not reach the central part of the gyre, where the studied core is located, because the material is transported further to the south by lateral currents of the gyre (Yasuda et al., 2014).

3. Materials and methods

3.1. Sediment core

A piston core MR0604-PC7A (51°16′56N, 149°12′60E and water depth of 1247 m) (Fig. 1) (hereafter called PC7A) was obtained at the central region of the Okhotsk Sea during MR06-04 of R/V Mirai, JAMSTEC, which took place in 2006. This site is bathed by PDW and above the present day carbonate compensation depth, located at approximately 1800 m water depth in the central Okhotsk Sea (Barash et al., 2008). This site was selected for a high-resolution multi-proxy analysis because it shows a clear lithological variation associated with the last Interglacial, good carbonate preservation and relatively high sedimentation rates. Sediments from the MIS 5e and bordering time intervals were analysed geochemically at high resolution in this core. The studied section has 2.25 m length, between 5.8 and 8.05 m depth. The sediments mainly consist of homogenous greyish olive diatom ooze and diatomaceous clayey silt with abundant ice-rafted debris (IRD).

Soft X-ray photographs were taken for the studied sections on-board using a SOFTEX PRO-TEST 150 to examine sedimentary structures, microstructures and IRD abundance. Voltages ranging from 40 to 50 kVp, currents from 2 to 3 mA and irradiation time from 150 to 200 s were used to optimize photographic conditions.

Total organic carbon (TOC) and nitrogen were measured in the studied section every 10 cm. After decalcification of the samples with 6 M HCl, both parameters were obtained by combustion at 1050 °C using a Heraeus CHN-O Rapid Elemental Analyzer as described by Müller et al. (1998). The C/N ratio was calculated with these data.

Isotopic analyses (C and O) were carried out using tests of the benthic foraminifera *Uvigerina* spp. with a 10 cm depth interval. Picked foraminifera tests were analysed with a GV IsoPrime mass spectrometer using an automated carbonate preparation system (IsoPrime Multiprep) at JAMSTEC. Each analysis represents a set of approximately 10 individuals, between 250 and 300 μm in diameter that were cleaned in an ultrasonic bath. The external precision is ~ ± 0.06‰.

Aluminum (Al), calcium (Ca) and silica (Si) concentrations were

measured using a non-destructive X-ray Fluorescence (XRF) scanner "TATSCAN-F2" (JAMSTEC), designed for quick 2-dimensional elemental imaging and scanning of sediment and rock surfaces (Sakamoto et al., 2006). In this study, u-channel samples were scanned with a 7 mm measurement diameter at 1 cm depth interval. A geological standard sample of JSd-2 (Imai et al., 1996) provided by the Geological Survey of Japan (AIST) was routinely measured before each section was run. Known errors in the data, including measurement errors derived from non-uniform sample surfaces and voids (fractures) in the U-channel, were manually removed.

Trace elements (Sc, Co, Ni, Cu, Rb, Sr, Y, Zr, Nb, Cs, Ba, Hf, Ta, Tl, Pb, Th, and U) were analysed using an Agilent 7500ce by inductively coupled plasma mass spectrometry (ICP-MS) (Agilent Technologies, Tokyo Japan) fitted with perfluoroalkoxy (PFA) sample introducing and Pt-inject torch each 2 to 5 cm. The ICP-MS was operated at no collision gas and multi-tune acquisition mode. This combination of the system allowed a wide range of elements be precisely determined using pulse counting detector, and also fluoric acid containing sample solution be delivered directly into plasma. Sample dissolution, preparation and measurement were described in Chang et al. (2003) and Nakamura and Chang (2007). Analytical accuracy and precision for ICP-MS analyses, estimated from repeated measurements of international reference rocks (JB-1a of the Geological Society of Japan (GSJ), BCR-2 and BIR-1 (Jochun et al., 2005) of the United States Geological Survey) were mostly better than 5% and 2–3%, respectively.

3.2. Used proxies

Different geochemical and mineralogical ratios have been used as paleoclimatic and paleoenvironmental proxies. Ca, Si and Ba-variations (Fig. 2) have been related to paleoproductivity in the studied region (e.g., Gorbarenko et al., 2007). The Ba/Al ratio and its equivalent Ba/Th ratio have been clearly associated with marine productivity in the Okhotsk Sea (e.g., Gorbarenko et al., 2007; Goldberg et al., 2005) and in other regions (Paytan et al. 1996). In the Okhotsk Sea massive barite deposits have been described associated to cold seeps (Greinert et al., 2002) but the cold seeps influence is very local and do not affect the studied location.

Si and Ca content in sediments are often associated with productivity in marine environments (e.g., presence of diatoms and calcitic or aragonitic organisms), but during low productivity periods particularly Si is controlled by the siliciclastic material. For a first-order discrimination between biogenic and detrital Si, we made a simple calculation of Si-excess, i.e. the non-siliciclastic Si, which we assume is identical to biogenic silica (Si biog.). This calculation is based on the assumption of an (idealized) pure siliciclastic end member, which is represented by the Si/Al ratio of the measurement with the highest Al counts (Fig. S1 in the supplement), with Al being a purely siliciclastic element. The deviation of total Si counts from the slope (with the assumption of a zero-intercept) is a maximum estimate of Si-excess (Si biog.). The high correlation between obtained Si biog. and the color parameter b^* (from blue to yellow), described as robust opal content proxy in Okhotsk Sea (Nürnberg and Tiedemann, 2004), corroborates the Si biog. interpretation and geochemical data base quality (Fig. S2). The Ca/Si ratio indicates decoupling between sources for Si and Ca, which would point to predominance of calcitic versus siliceous microfossils. Microscopic and smear slide observations confirm the presence of calcitic organisms, represented by coccolithophorids, when we reach high Ca/Si values, and the predominance of siliceous microfossils when Si increases, has already been described by previous studies (Sorokin and Sorokin, 1999; Broerse et al., 2000a, 2000b; Seki et al., 2007).

Stable isotope (C and O) composition from benthic foraminifera has been used as a proxy of water column conditions and age model support. It is well known that $\delta^{18}O$ in benthics mainly reflect changing glacial ice volumes and bottom waters generation (Rogerson et al., 2004). Nevertheless, variations in $\delta^{13}C$ are more complex and can reflect changes in water masses boundaries, ocean-atmosphere carbon equilibration, nutrient concentration and biological productivity, variations in the degree of stratification of the water column, upwelling activity or changes in the partitioning of $\delta^{13}C$ within the various components of the global carbon reservoir among other factors (e.g., Zahn et al., 1986; Mackensen et al., 1993; Herguera et al., 2010).

The C/N ratio is an useful proxy in order to decipher the provenance of the bulk organic matter from the sediments. C/N ratio values below 10 suggest a marine algal origin, and values above 20 continental vascular plants; intermediate values indicate a mixed source (Meyers 1994; 1997; Meyers and Teranes, 2001).

U/Th can be used as proxies for paleo-redox conditions and ventilation processes (e.g., Gallego-Torres et al., 2007). Changes in oxidation states promote variations from soluble U (VI) to immobile U (IV) (Anderson, 1982; Barnes and Cochran, 1990; Mangini et al., 2001). Organic substances also increase U content linked to the formation of organo-mineral compounds (Balistrieri and Murray, 1986). U/Th values between 0.75 and 1.25 have been related with dysoxic conditions and those higher than 1.25 with anoxia (Gallego-Torres et al., 2007).

On the other hand, Th/Sc, La/Yb and Eu anomalies have been interpreted as detrital proxies in different environments (e.g., Jimenez-Espejo et al., 2014; Gaiero et al., 2004; Shigemitsu et al., 2007; among others). The La/Yb ratio represents the whole Rare Earth Elements (REE) pattern and allows discriminating sedimentary, metamorphic, basalts and felsic rocks (Rollinson, 1993). The La/Yb and equivalent La/Lu ratio has been specifically used to discriminate aeolian inputs of the African craton from those of the European margin (Hamroush and Stanley, 1990) and aeolian input (loess) in the nearby Bering Sea (Shigemitsu et al., 2007). On the other hand, the Th/Sc ratio has been related to the acidity degree of the materials from the source area (being higher in granitic materials). Th is concentrated in acid igneous rocks, whereas the highest Sc contents are typical of more basic materials. The Th/Sc ration in this region has been interpreted to represent aeolian input (Shigemitsu et al., 2007), and higher Th/Sc values represent higher loess content. It further serves as a continental provenance proxy (Levitan and Lavrushin, 2009; Maslov et al., 2004) because acid rocks could indicate an increasing southern influence from the Kurile Islands (with a mix of rhyolitic and andesitic materials) versus those from the continent massifs bordering the northern Sea of Okhotsk (Levitan and Lavrushin, 2009).

The Eu anomaly (Eu^*) (Eu^* = (Eu sample/Eu chondrite)/(Sm sample/Sm chondrite)) is a parameter that is sensitive to the nature of detrital input (Gaiero et al., 2004). The average value of Eu^* in geologic regions around Okhotsk Sea are associated to diatom ooze (0.35) and granites (0.35), while the magmatic sequences of the western Kamchatka show intermediate values around 0.61, slightly lower than eastern Kamchatka (0.82), and highest values are associate to Island Arc sequences (0.93–1.10) (Levitan et al., 2007; Levitan and Lavrushin, 2009).

The obtained proxies have been compared with low resolution branched isoprenoid tetraether (BIT) index and paleo-SST proxy (TEX_{86}) data published previously by Seki et al. (2009), from site MR0604-PC7B (51°16′55N, 149°12′57E and water depth 1256 m) recovered in a very adjacent location during the same cruise. The BIT index is an indicator of the relative contribution of soil-derived GDGTs to marine GDGTs, and TEX_{86} (TetraEther indeX of tetraethers consisting of 86 carbon atoms) is a paleo-SST proxy, which is based on the number of cyclopentyl moieties in the isoprenoid glycerol dialkyl glycerol tetraether (GDGT) lipids (Schouten et al., 2002; Seki et al., 2009; 2014). TEX_{86}-derived SSTs have a reported error of ± 1.7 °C in the Okhotsk Sea (Seki et al., 2014)

3.3. Age model and sedimentation rate

Different penultimate interglacial period compilation studies demonstrate how complex and critical is the age model construction for

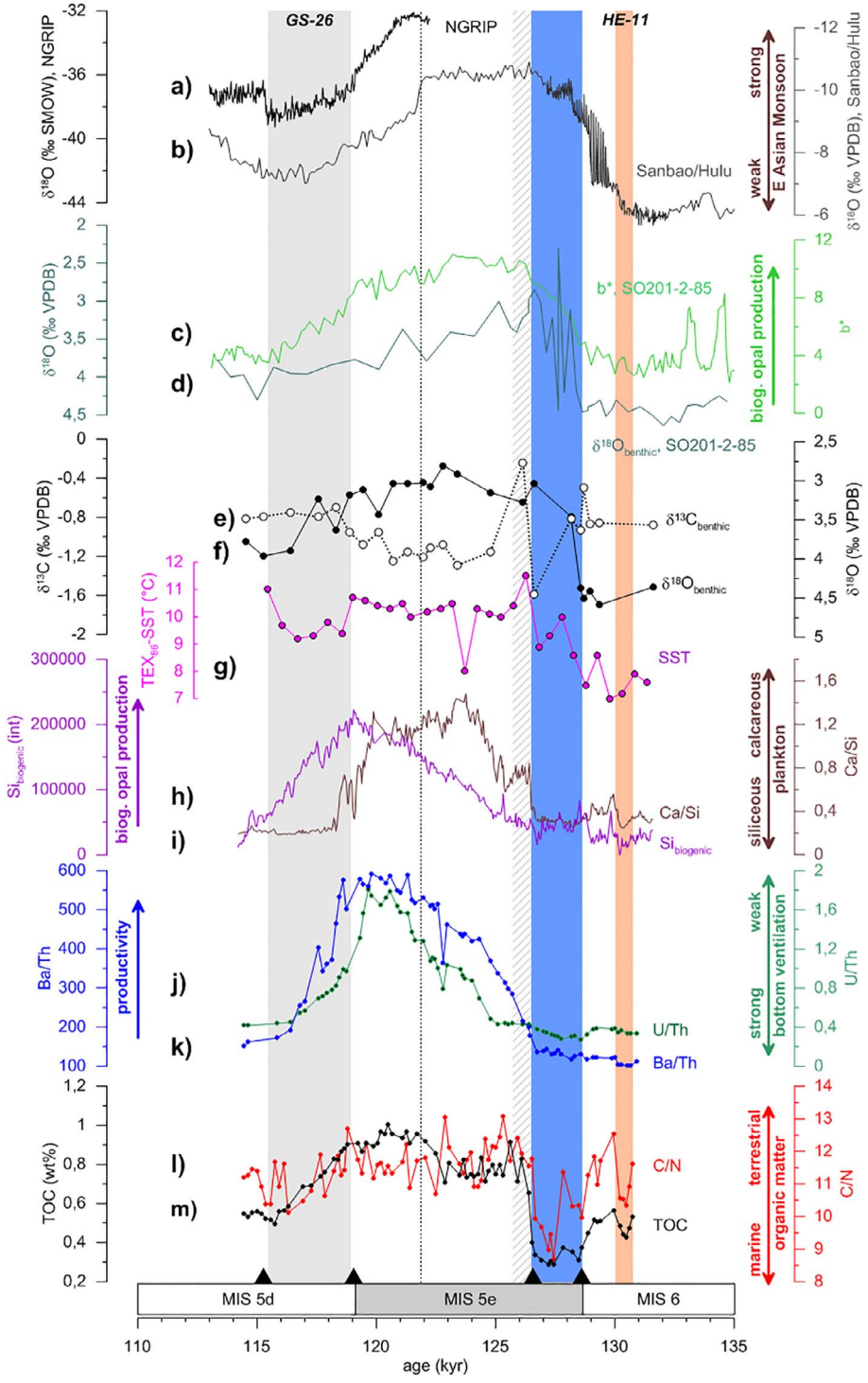

Fig. 2. Correlation of sediment core MR0604-PC7A age profiles and proxy interpretation with (a) $\delta^{18}O$ record (‰ SMOW) of the synthetic Greenland ice core (Barker et al., 2011); (b) Sanbao/Hulu stalagmite $\delta^{18}O$ records (Wang et al., 2001, 2008); (c) Core SO201-2-85 color b^* (Riethdorf et al., 2013), located in Western Bering Sea; (d) Core SO201-2-85 benthic $\delta^{18}O$ record from *Uvigerina peregrina*. Core MR0604-PC7A; (e) benthic $\delta^{13}C$ record from *Uvigerina* spp.; (f) benthic $\delta^{18}O$ record *Uvigerina* spp.; (g) Core MR0604-PC7B TEX_{86} –derived paleo Sea Surface Temperatures (Seki et al., 2009); (h) Core MR0604-PC7A Si biogenic record estimated from XRF-data; (i) Ca/Si ratio; (j) U/Th ratio; (k) Ba/Th ratio; (l) C/N ratio in organic matter; (m) Total organic matter content (wt%). Black triangles represent used age model tie points. Colored bars identify Heinrich 11 period (yellow), early MIS 5e period (blue and dashed bar), and Greenland Stadial 26 (gray). (For interpretation of the references to color in this figure legend, the reader is referred to the web version of this article.)

this period (Capron et al., 2017; Hoffman et al., 2017). At the studied region Gorbarenko et al. 2017 described that age model for this period has been constructed at least by four methods: (i) astronomical calibration of colour parameters and lithological changes (e.g., site MD01-2415, Nürnberg and Tiedemann, 2004), (ii) graphic correlation of productivities proxies (Gorbarenko et al., 2010; 2017); (iii) correlation of b^* values with previous Okhotsk sea dated cores (Khim et al., 2012) and (iv) correlation of the benthic $\delta^{18}O$ isotopic record with the global benthic $\delta^{18}O$ stack LR04 (Lisiecki and Raymo, 2005) (Sugisaki et al., 2010). In addition, paleomagnetic studies in this region demonstrate that is a useful tool for age model construction and inter-core correlation (Inoue and Yamazaki, 2010; Yamazaki et al., 2013).

The age modelling for the PC7A chronostratigraphic approach for ages < 100 kyr is robust and includes high-resolution core logging data (magnetic susceptibility), benthic $\delta^{18}O$ stratigraphy and luminescence dating for absolute age control (Seki et al., 2009; Sugisaki et al., 2010). The errors of age control points derived from luminescence data in sediments older than 100 kyr are too big for its effective use, and age models based on tuning a low resolution benthic foraminiferal $\delta^{18}O$ record (Seki et al., 2009; Sugisaki et al., 2010) to the global LR04 stack (Lisiecki and Raymo, 2005) provided insufficient age control. In this study we used a different age model to those previously presented that also include a correlation between productivity proxies (colour reflectance b^* and Si biog.) and well dated sequences in the western

Table 1
Age-depth points for core MR0604-PC7A model.

Core/Section	Depth (cm)	Kyr cal. BP	Approach
PC07A/4 82-88	319	101 ± 5	OSL absolute date (Sugisaki et al., 2010)
PC07A/6 13-15	449	115.3	Si bio-b* Vs b* (Riethdorf et al., 2013)
PC07A/6 61-63	490	119.0	Si bio-b* Vs b* (Riethdorf et al., 2013)
PC07A/7 53-55	589	126.6	δ^{18} benthic Vs δ^{18} benthic (Riethdorf et al., 2013)
PC07A/7 83-85	619	128.6	δ^{18} benthic Vs δ^{18} benthic (Riethdorf et al., 2013)

Bering Sea (core DO201-2-85KL, 57°30.30′N; 170°24.77′E), (Riethdorf et al., 2013) and the Sanbao/Hulu stalagmite δ^{18}O record (Wang et al., 2008) (Fig. 2a–d). The main discrepancy between the age model previously published in (Seki et al., 2009; Sugisaki et al., 2010) and the new PC7A chronostratigraphy is related to the large offset between the LR04 and Sanbao/Hulu records for the Termination II age and the different isotopic/event age attribution. In this study we assume that we will experience similar benthic δ^{18}O influences/changes through time in both records as well as synchronous productivity changes. Hence, we have assigned tie points at 128.6, 126.6, 119.0 and 115.3 kyr based on the benthic δ^{18}O record, defining the MIS 5e plateau in productivity and SST (Table 1). Age models based on 4 tie points are common for the MIS 5e studies (e.g., Irvali et al., 2012) and the difference with near locate records e.g., Gorbarenko et al. 2017 is ± 1.0 kyr. Ages between the control points were calculated by interpolation assuming constant sedimentation rate. The resulting age model results in a mean sedimentation rate of 10.5 cm/kyr for the MIS 5e productivity plateau (from aprox. 124 to 119 kyr, based in Ba/Th ratio).

Average temporal resolution of XRF scanner samples is 40 yr and between 150 and 400 yr for other analysis, which allows us to distinguish millennial/centennial climate oscillations. Although the absolute uncertainty of the constructed age model is likely few thousand years, the MIS 5e plateau is recognized and is pertinent to discuss millennial scale variations and the sequence of consecutive events, especially these variations that are prominent in the high resolution XRF scanner data.

4. Results and discussion

4.1. The MIS 6 final stage

The sediment in core PC7A during glacial MIS 6 is mainly composed of quartz, feldspars, clay minerals and plagioclase from the surrounding emerged lands (Harada, 2006). Obtained X-ray images indicate the existence of IRD included in the sediment during this period (Fig. S3). The existence of IRD in marine sediments has been attributed to seasonal and/or multiannual ice melting, because IRD deposition does not take place under perennial-ice condition (e.g., in the central Arctic Sea) because terrigenous grains are trapped (Sakamoto et al., 2005). In addition, TEX_{86}-deverived temperature from a nearby site indicate paleo-SST between 7 and 9 °C (Seki et al., 2009), all pointing to non-perennial ice conditions in the central Okhotsk during MIS 6, despite the northwestern sector being covered by annual sea-ice during glacial times (Gorbarenko et al., 2003; Yamazaki et al., 2013).

The detrital material during glacial periods was transported to the entire Okhotsk Sea by ice as IRD, ocean currents, aeolian, and fluvial processes (Sakamoto et al., 2005). In the case of the central Okhotsk Sea, the Amur River supply is not important, taking into account the current ocean configuration and lower river discharge during glacial conditions (Liu et al., 2006; Yasuda et al., 2014). In order to discern between continental and aeolian input, previous authors estimated end-member compositions based in Th/Sc and La/Yb ratios, proposing a signal derived from Kurile-Kamchatkan (K-K) volcanic material and from loess in the North Pacific realm (Weber et al., 1996; Otosaka et al., 2004; Shigemitsu et al., 2007). The obtained data at site PC7A (Fig. 3) has been compared with these end members and almost all are located on or a little above the mixing line (Fig. 4). Our results indicate that loess content was higher during the MIS 6 periods (Th/Sc > 0.4) in agreement with studies that describe high loess input in the mild-latitudes of the western North Pacific during glacial periods (e.g., Kawahata et al., 2000). Our data further imply a decrease of loess input during the early MIS 5e (Fig. 3c). Notably, variations in the loess signal do not affect the Eu* values. The Eu* values around 0.63 (Fig. 3d) indicate that granitic material from western Kamchatka is also a main detrital source during MIS 6 in the fine fraction. Nevertheless a study based in drop stones at southern site OS03-1 indicates also the influence of Eastern Kamchatka input in the coarse fraction (Wang et al., 2017).

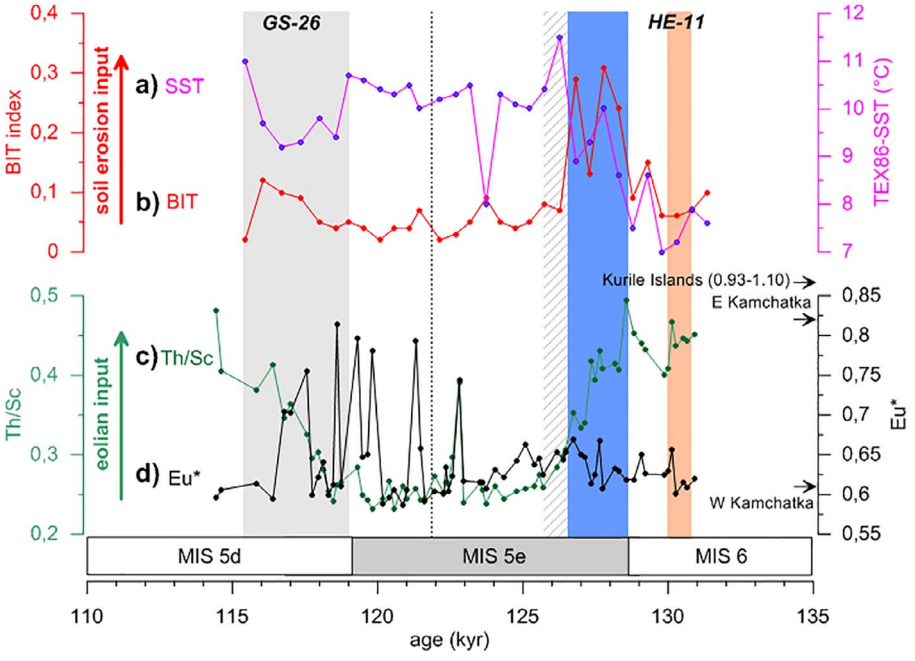

Fig. 3. Core MR0604-PC7B age profiles (Seki et al., 2009) of: (a) BIT index, an indicator of the relative abundance of soil GDTTs relative to marine GDGTs; (b) TEX_{86} –derived SST compared with core MR0604-PC7A; (c) Th/Sc ratio; (d) Eu anomaly. Arrows represent Eu* values for different regions from Levitan and Lavrushin, 2009.

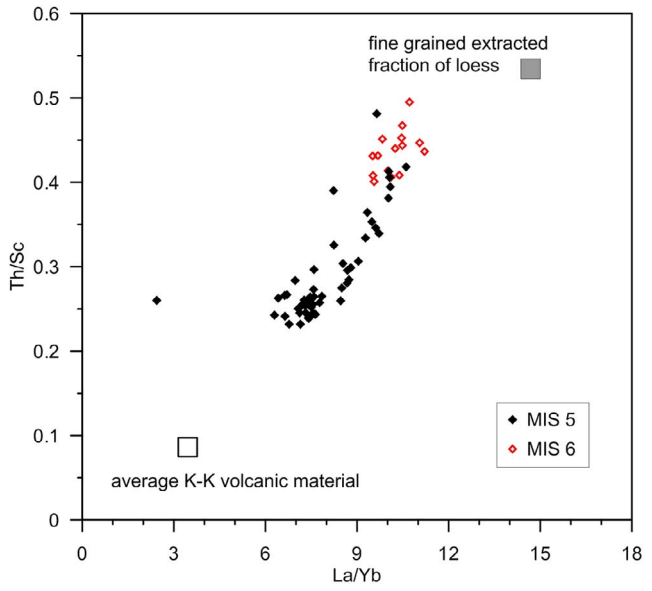

Fig. 4. Scatter plots of Th/Sc versus La/Yb at core MR0604-PC7A. Red dots represent MIS 6 values and black dots those corresponding to MIS 5. Squares represent previously described Kurile-Kamchatka and loess material Th/Sc and La/Yb end-members.

Obtained difference could be linked with variable composition between bulk and coarse fractions.

Low Ba/Th and U/Th ratios (Fig. 2j, k) indicate low productivity and well oxygenated conditions in agreement with previous studies that reconstruct glacial conditions (e.g., Keigwin, 1998). Our records also seems to be sensitive to the Heinrich 11 event (Oppo et al., 2006) (Fig. 2 pink bar), recognized by lower temperatures and a decrease in C/N ratios and TOC content, pointing to a decrease in productivity during cold periods during MIS 6.

The MIS-6 demise and the onset of the penultimate deglacial stage is a matter of controversy. Different studies propose the beginning of the interglacial MIS 5e from 135 to 142 kyr (e.g., Sugisaki et al., 2010; Thompson and Goldstein, 2006; Thomas et al. 2009). Nevertheless, we placed the onset of the MIS 5e at 128.6 kyr, parallel to maximum northern hemisphere summer insolation throughout the Northern Hemisphere (130–127 kyr) (Berger and Loutre, 1991), $\delta^{18}O$ record (‰ SMOW) of the synthetic Greenland ice core (Barker et al., 2011), Sanbao/Hulu (Wang et al., 2008) and site SO201-2-85 (57°30.30′N; 170°24.77′E, Bering Sea) color b^* parameter (Riethdorf et al., 2013) records (Fig. 2).

4.2. Early MIS-5e: deglaciation pattern

Oxygen isotopic composition (from 4.5 to 3‰) and paleo-SST (from 9 to 11 °C) show parallel variations during the early MIS 5e (Fig. 2f, g blue bar). Paleo-SST fluctuates and shows a see-saw trend during Termination II (Seki et al., 2009) mirrored by C/N ratios and the BIT index. This variability during the deglaciation-like period can be linked with a minor cooling in Europe (Sirocko et al., 2005). The coincident relative minima in these three proxies can be explained by variable cold fresh water pulses and likely major delivery of shelf preserved soil material (high BIT index) under prevalent marine productivity condition (low C/N ratio) (Fig. 3a blue bar). They may be linked to detrital supply events from the Kamchatka Peninsula, where extended mountain glaciers protruded down towards the sea, as was proposed for the end of the MIS-6 and the beginning of MIS-5e (Nürnberg et al., 2011). Obtained Eu^* values also agree with a W Kamchatka provenance during the MIS 6 and the early MIS 5e.

During this interval the Th/Sc ratio shows a continuous decreasing pattern (Fig. 3c). Variations in this proxy can indicate a decrease in loess input and variations in the detrital sources. Changes in dust sources from Siberia-Northeast China area to the Taklimakan Desert-Loess Plateau region have been described during this period for the Japan Sea (Nagashima et al., 2007) and a similar trend of decreasing aeolian input has been described in the western subarctic Pacific nearby Bering Sea (Shigemitsu et al. 2007). This parallelism in the loess supply in the entire northwestern Pacific realm during the penultimate glacial/interglacial transition suggests a major change in the atmospheric pattern in this region. As the supply of loess to these high latitudes depends on the monsoonal activity (An et al., 1991), a progressive increase of monsoonal strength during the penultimate deglaciation time could be expected, together with enhanced freshwater input from river and sea ice melting.

Despite all described changes during this deglaciation-like interval it is remarkable that the thermohaline circulation did not appear to be affected. No major changes were detected on productivity, oxygenation and water column conditions, according to the TOC, Ba/Th, and U/Th ratio records (Fig. 2j, k, m), and low productive and well-oxygenated conditions were sustained throughout the entire interval (Fig. 5a, b).

4.3. The middle MIS 5e (~126 to ~122 kyr): transient and calcium predominant marine productivity conditions

The values of Ba/Th and U/Th show a large increase at ~126.5 and 125 kyr (Fig. 2j, k). These results can be interpreted as a dramatic increase in productivity and increasing bottom water oxygen depletion in the central Okhotsk Sea. This major change is coeval with a retreat of sea ice, decreasing IRD abundance in the region (Gorbarenko et al., 2017), and a stabilization of the sea level increase (Thomas et al., 2009). We propose that this event can also be traced in records from other Artic regions as the Nordic seas, where the warmest sea surface temperatures were reached (Knudsen et al., 2002). This ~3-kyr lag of the Okhotsk productivity increase to the benthic $\delta^{18}O$ increase, and rising radiative forcing, is similar to the estimated lag between the insolation maximum and monsoonal dynamics deposits in the North Hemisphere (e.g., Ziegler et al., 2010) and to the retreat of marine based ice sheets (Carlson and Winsor, 2012). Persistent cold conditions during the early MIS 5e also have been described in other Artic and subarctic records (e.g., Bauch et al., 2011; 2012). A muted response to orbital forcing during the MIS 5e also reconstructed in the Artic Circle Far East Russia El'gygytgyn lacustrine record (Melles et al., 2012) compared with previous interglacial periods (MIS 11 and 31). The origin of the distinct persistence of glacial conditions in the Arctic region is not clear, but might be linked with reduced northern North Pacific upwelling (Hall et al., 2001) or other processes and feedbacks including greenhouse gas forcing (Melles et al., 2012).

The prominent variation in the Ca/Si ratio at ~126 kyr indicates an important transient period (Fig. 2i dashed bar). The Ca/Si ratios clearly mark a switch to dominant $CaCO_3$ accumulation relative to opal contents, equivalent to the one previously reported during recent deglaciations (Sato et al., 2002; Khim et al., 2012). The origin of this carbonate accumulation is under debate. It has been linked to poor nutrient supply (Si) caused by strong stratification (Sato et al., 2002; Khim et al., 2012; Iwasaki et al., 2012) or to a better carbonate preservation promoted by changes in ventilation as occurred during the last deglaciation (Okazaki et al., 2014). Redox proxies (e.g., U/Th) do not indicate an increase in bottom sea dysoxia (Fig. 2j), while paleo-SST and aeolian dust tracers indicate warmer temperatures and lower aeolian input (Fig. 2g, 3c). C/N ratio also indicate an increase in continental organic matter input from 126 kyr, all in agreement with an enhance monsoonal activity and therefore, a dominance of warm and moist air masses over the Amur River catchment basin and Okhotsk Sea, which would imply a change in the thermohaline conditions (Harada et al., 2006, 2008). All these evidences point to a change in the nature of the surface and deep-water masses as the driving factor for carbonate preservation instead of stratification (Fig. 5c). We can expect a major

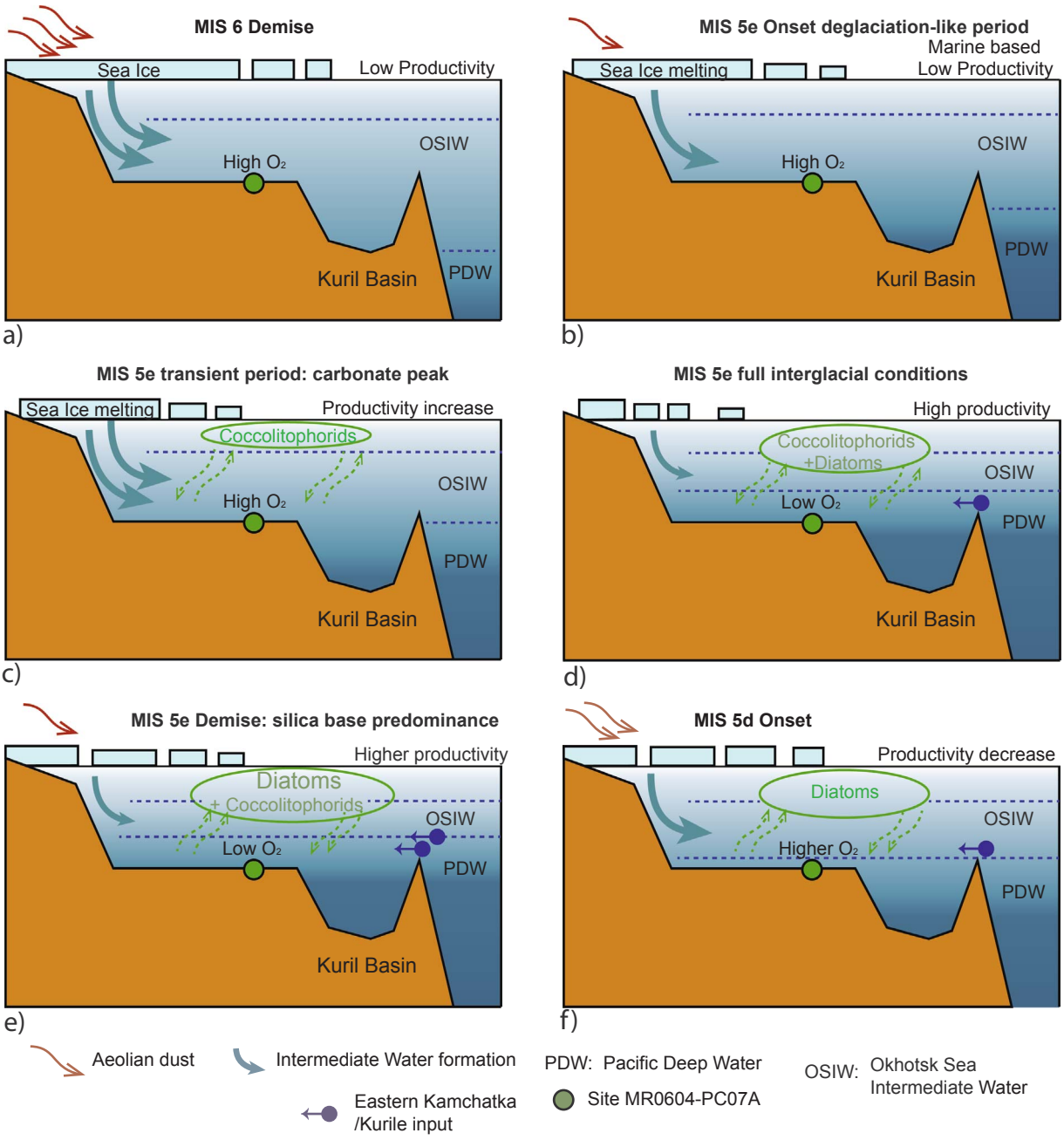

Fig. 5. Schematic representation of atmospheric and oceanographic conditions recorded at core MR0604-PC7A during described periods organized by consecutive time slides (modified from Iwasaki et al., 2012). OSIW: Okhotsk Sea Intermediate Water, PDW: Pacific Deep Water.

influence of this transient episode in the North Pacific Intermediate Waters as described for the last deglaciation (e.g., Max et al., 2014).

After this transient period we observed an increase in silica biogenic (Fig. 2h) and, despite the clear increase in productivity (Fig. 2m), we find lighter and stable benthic $\delta^{13}C$ values (Fig. 2f). Previous studies in the NW Pacific already detected a deglacial lowering of $\delta^{13}C$ coincident with deposition of diatomaceous facies, attributed to increased biological productivity (Keigwin et al., 1992) or/and mass water changes (Keigwin, 1998). $\delta^{13}C$ values decline to $\sim -1.2‰$, pointing to the presence of poorly ventilated and nutrient-rich water masses. This decline could be explained by water masses changes or organic matter accumulation. The replacement of OSIW by a water mass with light $\delta^{13}C$ values (Fig. 5d), e.g., PDW with $\delta^{13}C$ values of $\sim -0.8‰$ (Fig. 2e), can explain this variation (Takahashi et al. 2000b). This lowering of benthic foraminiferal $\delta^{13}C$ below that of ambient bottom water could be also induced by an isotopically light microenvironment through organic matter oxidation (Zahn et al., 1986; Mackensen et al., 1993) or more likely to a different composition of the Glacial-PDW (Adkins et al., 2002). Nevertheless, water mass replacement appear more plausible because diatoms blooms also indicate PDW presence, because these are silica rich waters fostering diatom presence, while siliceous plankton growth is prevented during glacial periods by the expansion of Si-poor OSIW (Fig. 5d) (Iwasaki et al., 2012).

Another evidence for water mass replacement is linked with the significant increase in U/Th showing reducing bottom water conditions from ~124 kyr (dysoxic conditions; U/Th > 0.75). At ~121.5 kyr U/

Th ratios reach values > 1.25 that has been associated to anoxia (Gallego-Torres et al., 2007), nevertheless, the continuous presence of benthic foraminifera indicates rather dysoxic conditions (oxygen concentrations of 0.3–0.1 ml/l) (Psheneva and Gorbarenko, 2013). The two primary factors controlling dissolved-oxygen concentration in and below the sediment-water interface are a high biological productivity and/or poor water ventilation. At our study site, productivity peaks (e.g. Ba/Th, TOC, Si biog.) correlate well with the lowest bottom oxygenation levels (U/Th) (Fig. 2h, k, j, m), pointing to productivity as major forcing, an equivalent phenomena to present days conditions (Salyuk et al., 2003).

4.4. The MIS 5e demise: silica predominant marine productivity

During the late MIS 5e productivity proxies (Ba/Th) and dysoxia (U/Th) reached maximum values, Si biog. increases and Ca/Si ratio decline (Fig. 2 line dotted). Nevertheless, at ~120 kyr these variations in productivity were not linked with the increase in oxygenation conditions (Fig. 2j) and heavier $\delta^{13}C$. This shows the influence of deep-water masses on bottom water oxygen state and points towards a progressive replacement of poor oxygenated PDW by OSIW, completed during the glacial stage (GS) 26 at central Okhotsk Sea. Although all these changes took place during a relatively weak East Asian Monsoon (Fig. 2b), Th/Sc ratios related to aeolian input do not indicate any kind of variation (Fig. 3) while Eu* showed a wider range (from 0.58 to 0.81) during the late MIS 5e. These higher values suggest occasional inputs from Eastern Kamchatka or the Kurile Islands, according to Levitan and Lavrushin (2009). This interpretation agrees with the proposal of Gorbarenko et al. (1996), suggesting that continental ice sheets were not developed in eastern Siberia, and the main source of meltwaters was the ice sheet and icebergs from Kamchatka.

During this late MIS 5e period, our SST record indicates a slightly warming (Fig. 2 g). However, we propose that maximum productivity conditions in this Okhotsk sea region are linked to a higher input of PDW instead to SST variations.

4.5. The early MIS 5d

The end of the last interglacial period and its glacial inception is debated. It has been placed around 116 and 113 kyr (Stirling et al., 1998; Muhs et al., 2002) in agreement with relatively low summer insolation values (Berger and Loutre, 1991). Nevertheless other authors placed the age of the upper boundary of the MIS 5e at ~111 kyr (Bauch et al., 2012). In our record the end of the MIS 5e has been placed at ~119 kyr following the INTIMATE event stratigraphy (Rasmussen et al., 2014). Here our data indicates a marked productivity decrease and the benthic $\delta^{13}C$ values show a trend towards heavy values (Fig. 2f, k). The paleo-SST record also indicates a cooling, and it can be correlated with the established GS-26 cooling (Rasmussen et al., 2014) in agreement with close records (Gorbarenko et al., 2017).

Organic matter provenance proxies (e.g., C/N ratio) show a variation but Ca/Si, U/Th suffers abrupt changes, and $\delta^{13}C$ progressively increases compared with the MIS 5e level (Figs. 2 and 3). These variations can be explained by a modified water column configuration. Site PC7A data allow us to discriminate that stratification was becoming weaker with the U/Th ratio indicating that dysoxic conditions decreased at ~119 kyr and that full oxic conditions were re-established during early MIS 5d. Increase in oxygenation is mirrored by the increase in $\delta^{13}C$ likely promoted by mixing of PDW with intermediate waters (Fig. 5f). This intensified ventilation in the Okhotsk Sea can be related to a decrease in freshwater supply (less precipitation and less riverine inputs), and increasing salinity in agreement with a weaker monsoonal activity and reduced supply of silicate. Reduced silicate input is also supported by low Ca/Si indicating a near-absence of coccolithophorids and other carbonaceous phytoplankton and a predominance of siliceous microplankton. These changes bear great similarity to those described during the middle-late Holocene (Seki et al., 2004; Iwasaki et al., 2012; Khim et al., 2012).

Eu^{*} still shows a considerable scatter with high values pointing to a clear influence from Eastern Kamchatka and the Kurile Island. Proxies associated with aeolian input do not show significant variations (Fig. 3), pointing to variations in other Okhotsk Sea regions as the main driver for thermohaline circulation in the entire basin, like sea ice formation in the northwest Okhotsk Sea.

With the onset of MIS 5d benthic $\delta^{13}C$ reaches MIS 6 values (Fig. 2e) reflecting the complete replacement of PDW by OSIW, however, productivity (Si biog.) appear to be still relatively high during GS-26 (Fig. 5f). Higher Th/Sc values indicate an increase in aeolian input and Eu^{*} values show a progressive reduction of detrital input from the southern Kurile Islands. The studied proxies indicate that at the GS-26 kyr full glacial conditions were reached.

5. Conclusions

Geochemical proxies show evidence for significant paleoenvironmental changes in the central Okhotsk Sea during the penultimate interglacial period. Obtained data confirm previous studies that indicate glacial/interglacial and millennial scale changes in warm/cold conditions affected productivity (as can be interpreted from C/N ratio and TOC data). Nevertheless, for the first time we describe in detail the relationship between changes in the water column structure, eolian input and shifts in the provenance of detrital material during MIS 5e. We further propose three phases for the MIS 5e mainly based on paleoproductivity variations.

The start of the MIS 5e evolves in a deglaciation-like mode, characterized by a decrease in aeolian input, variations in the organic matter sources with only minor changes in the water column properties. We observe an offset between the increase in productivity and $\delta^{18}O$ benthic isotopic variations that indicate a certain resilience of sea ice to radiative forcing compared with other regions.

A transitional period associated to a carbonate peak and water column instability can be distinguished before reaching the MIS 5e productivity plateau. The carbonate peak appears to be linked with deep convection, appearances of PDW and carbonate preservation.

During the MIS 5e geochemical productivity plateau we distinguish two periods: one dominated by carbonate productivity and another one with silica preponderance and higher contribution of detrital material from the Kurile Islands and Eastern Kamchatka. These changes during the MIS 5e full interglacial conditions can be explained by the presence of PDW in the central Okhotsk Sea, high marine productivity and a decrease in monsoonal activity.

The early demise of MIS 5e at ~120 kyr is accompanied by water column variations similar to those described for the middle Holocene. These involved intense water column mixing, decrease in carbonate nannofossil content and increase in bottom water ventilation. The MIS 5e to MIS 5d transition is characterized by an increase of aeolian input, complete replacement of PDW by OSIW, predominance of silica based marine productivity and cold sea surface temperatures. After the GS-26 period typical glacial conditions were reached.

Acknowledgments

We are grateful to the crew of R/V Mirai for their help with sediment collection during the MR06-04 cruise. We want to thank to Dr. Tatsuhiko Sakamoto for using the instruments XRF-Scanner (Tatscan F-2). The authors are indebted to Dr. Zhou as editor and two anonymous reviewers for their invaluable comments and reviews. This work was partially supported by the Japan Agency for Marine-Earth Science and Technology and Ministry of Education, Culture, Sports, Science and Technology Japan. A.G.-A. was also supported by a Ramón y Cajal Fellowship RYC-2015-18966 of the Spanish Government (Ministerio de Economía y Competividad).

Appendix A. Supplementary material

Supplementary data associated with this article can be found, in the online version, at https://doi.org/10.1016/j.jseaes.2018.01.032.

References

Adkins, J.F., Mcintyre, K., Schrag, D.P., 2002. The salinity, temperature, and $\delta^{18}O$ of the glacial deep ocean. Science 298, 1769–1773.

An, Z.S., Kukla, G., Porter, S.C., Xiao, J.L., 1991. Magnetic susceptibility evidence of monsoon variation on the loess plateau of central China during the last 130,000 years. Quat. Res. 36, 29–36.

Anderson, R.F., 1982. Concentration, vertical flux, and remineralization of particulate uranium in seawater. Geochim. Cosmochim. Acta 46, 1293–1299.

Barker, S., Knorr, G., Edwards, R.L., Parrenin, F., Putnam, A.E., Skinner, L.C., Wolff, E., Ziegler, M., 2011. 800,000 years of abrupt climate variability. Science 334, 347–351.

Balistrieri, L.S., Murray, J.W., 1986. The surface-chemistry of sediments from the panama basin – the influence of Mn oxides on metal adsorption. Geochim. Cosmochim. Acta 50, 2235–2243.

Barash, M.S., Khusid, T.A., Matul, A.G., Chekhovskaya, M.P., Biebow, N., Nürnberg, D., Tiedemann, R., 2008. Distribution of benthic foraminifera in upper Quaternary sediments of the Deryugin basin (Sea of Okhotsk). Oceanology 48, 105–113.

Barnes, C.E., Cochran, J.K., 1990. Uranium removal in oceanic sediments and the oceanic U balance. Earth Planet. Sci. Lett. 97, 94–101.

Bauch, H.A., Kandiano, E.S., Helmke, J., Andersen, N., Rosell-Mele, A., Erlenkeuser, H., 2011. Climatic bisection of the last interglacial warm period in the Polar North Atlantic. Quat. Sci. Rev. 30, 1813–1818.

Bauch, H.A., Kandiano, E.S., Helmke, J.P., 2012. Contrasting ocean changes between the subpolar and polar North Atlantic during the past 135 ka. Geophys. Res. Lett. 39, L11604.

Berger, A.L., Loutre, M.F., 1991. Insolation values for the climate of the last 10 millions years. Quat. Sci. Rev. 10, 297–317.

Broerse, A.T.C., Ziveri, P., Honjo, S., 2000a. Coccolithophore (–$CaCO_3$) flux in the Sea of Okhotsk: seasonality, settling and alteration processes. Mar. Micropaleontol. 39, 179–200.

Broecker, W., 1991. The great ocean conveyor. Oceanography 1, 79–89.

Broerse, A.T.C., Ziveri, P., Honjo, S., 2000b. Coccolithophore (–$CaCO_3$) flux in the Sea of Okhotsk: seasonality, settling and alteration processes. Mar. Micropaleontol. 39, 179–200.

Capron, E., Govin, A., Feng, R., Otto-Bliesner, B.L., Wolff, E.W., 2017. Critical evaluation of climate syntheses to benchmark CMIP6/PMIP4 127 ka Last Interglacial simulations in the high-latitude regions. Quat. Sci. Rev. 168, 137–150.

Carlson, A.E., Winsor, K., 2012. Northern Hemisphere ice-sheet responses to past climate warming. Nat. Geosci. 5, 607–613.

Chang, Q., Shibata, T., Shinotsuka, K., Yoshikawa, M., Tatsumi, Y., 2003. Precise determination of trace elements in geological standard rocks using inductively coupled plasma mass spectrometry (ICP-MS). Front. Res. Earth Evol. 1, 357–362.

Chebykin, E.P., Gorbarenko, S.A., Stepanova, O.G., Panov, V.S., Goldberg, E.L., 2015. Geochemical multielement signatures of glacial and interglacial facies of the Okhotsk Sea deepwater sediments during the past 350 kyr: a response to global climate changes at the orbital and millennial scales. Paleoceanography 30, 303–316.

Gaiero, D.M., Depetris, P.J., Probst, J.-L., Bidart, S.M., Leleyter, L., 2004. The signature of river- and wind-borne materials exported from Patagonia to the southern latitudes: a view from REEs and implications for paleoclimatic interpretations. Earth Planet. Sci. Lett. 219, 357–376.

Gallego-Torres, D., Martínez-Ruiz, F., Paytan, A., Jimenez-Espejo, F.J., Ortega-Huertas, M., 2007. Pliocene-Holocene evolution of depositional conditions in the eastern Mediterranean: role of anoxia vs. productivity at time of sapropel deposition. Palaeogeogr. Palaeoclimatol. Palaeoecol. 246, 424–439.

Goldberg, E.L., Gorbarenko, S.A., Shaporenko, A.D., Bosin, A.A., Leskov, V.Yu., Chebykin, E.P., 2005. Instability of last glacial climate from SRXFA data for bottom sediments in the Okhotsk Sea. Nucl. Instrum. Methods Phys. Res. A 543, 284–287.

Gorbarenko, S.A., 1996. Stable isotope and lithologic evidence of late-glacial and Holocene oceanography of the northwestern Pacific and its marginal seas. Quat. Res. 46, 230–250.

Gorbarenko, S.A., Chekhovskaya, M.P., Southon, J.R., 1998. About the paleoenvironment of the central part of Okhotsk Sea during the Last Glaciation and the Holocene. Oceanology 38, 305–308.

Gorbarenko, S.A., Leskov, V.Yu., Artemova, A.V., Tiedemann, R., Biebow, N., Nürnberg, D., 2003. Sea ice coverage of the Okhotsk Sea during last glacial and Holocene. Dokl. Earth Sci. 388, 678–682.

Gorbarenko, S.A., Goldberg, E.L., Kashgarian, M., Velivetskaya, T.A., Zakharkov, S.P., Pechnikov, V.S., Bosin, A.A., Psheneva, O.Yu., Ivanova, E.D., 2007. Millennium scale environment changes of the Okhotsk Sea during last 80 kyr and their phase relationship with global climate changes. J. Oceanogr. 63, 609–623.

Gorbarenko, S.A., Psheneva, O.Y., Artemova, A.V., Matul, A.G., Tiedemann, R., Nürnberg, D., 2010. Paleoenvironment changes in the NW Okhotsk Sea for the last 18 thousand years by micropaleontologic, geochemical, and lithological data. Deep-Sea Res. I: Oceanogr. Res. 57, 797–811.

Gorbarenko, S.A., Harada, N., Malakhov, M.I., Velivetskaya, T.A., Vasilenko, Y.P., Bosin, A.A., Derkachev, A.N., Goldberg, E.L., Ignatiev, A.V., 2012. Responses of the Okhotsk Sea environment and sedimentology on global climate changes at the orbital and millennial scale during the last 350 kyr. Deep-Sea Res. II 61–64, 73–84.

Gorbarenko, S., Velivetskaya, T., Malakhov, M., Bosin, A., 2017. Glacial terminations and the Last Interglacial in the Ohkotsk Sea; Their implication to global climatic changes. Global Planet. Change 152, 51–63.

Greinert, J., Bollwerk, S.M., Derkachev, A., Bohrmann, G., Suess, E., 2002. Massive barite deposits and carbonate mineralization in the Derugin Basin, Sea of Okhotsk: precipitation processes at cold seep sites. Earth Planet. Sci. Lett. 203, 165–180.

Hall, I.R., Carter, L., Harris, S.E., 2001. Intesnsified deep Pacific inflow and ventilation in Pleistocene glacial times. Nature 412, 809–811.

Hamroush, H.A., Stanley, A.D.J., 1990. Paleoclimatic oscillations in East Africa interpreted by analysis of trace elements in Nile delta sediments. Episodes 13, 264–269.

Harada, N., 2006. MIRAI cruise report MR06–04 Leg2. Japan Agency for Marine-Earth Science and Technology, Yokosuka. Available at < http://www.godac.jamstec.go.jp/cruisedata/mirai/e/MR06-04_leg1.html > .

Harada, N., Ahagon, N., Sakamoto, T., Uchida, M., Ikehara, M., Shibata, Y., 2006. Rapid fluctuation of alkenone temperature in the southwestern Okhotsk Sea during the past 120 ky. Glob. Planet. Change 53, 29–46.

Harada, N., Sato, M., Sakamoto, T., 2008. Freshwater impacts recorded in tetra-unsaturated alkenones and alkenone-SSTs from the Okhotsk Sea across millennial-scale cycles. Paleocenography 23 PA3201.

Hays, J.D., Morley, J.J., 2004. The Sea of Okhotsk: A window on the Ice Age ocean. Deep-Sea Res. Part I 51, 593–618.

Herguera, J.C., Herbert, T., Kashgarian, M., Charles, C., 2010. Intermediate and deep water mass distribution in the Pacific during the Last Glacial Maximum inferred from oxygen and carbon stable isotopes. Quat. Sci. Rev. 29, 1228–1245.

Hoffman, J.S., Clark, P.U., Parnell, A.C., He, F., 2017. Regional and global sea-surface temperatures during the last interglaciation. Science 355 276e279.

Hong, Y.T., Hong, B., Lin, Q.H., Shibata, Y., Zhu, Y.X., Leng, X.T., Wang, Y., 2009. Synchronous climate anomalies in the western North Pacific and North Atlantic regions during the last 14,000 years. Quat. Sci. Rev. 28, 840–849.

Imai, N., Terashima, S., Itoh, S., Ando, A., 1996. 1996 compilation of analytical data on nine GSJ geochemical reference samples, “Sedimentary rock series”. Geostand. Newsl. 20, 165–216.

Inoue, S., Yamazaki, K.I., 2010. Geomagnetic relative paleointensity chronostratigraphy of sediment cores from the Okhotsk Sea. Palaeogeogr. Palaeoclimatol. Palaeoecol. 291, 253–266.

Itoh, M., Ohshima, K.I., 2000. Seasonal variations of water masses and sea level in the Southwestern part of the Okhotsk Sea. J. Oceanogr. 56, 643–654.

Itoh, M., Ohshima, K.I., Wakatsuchi, M., 2003. Distribution and formation of Okhotsk Sea Intermediate Water: An analysis of isopycnal climatological data. J. Geophys. Res. 108, 3258–3276.

Iwasaki, S., Takahashi, K., Maesawa, T., Sakamoto, T., Sakai, S., Iijima, K., 2012. Paleoceanography of the last 500 kys in the central Okhotsk Sea based on geochemistry. Deep-Sea Res. II 61–64, 50–62.

Irvali, N., Ninnemann, U.S., Galaasen, E.V., Rosenthal, Y., Kroon, D., Oppo, D.W., Kleiven, H.F., Darling, K.F., Kissel, C., 2012. Rapid switches in subpolar North Atlantic hydrography and climate during the Last Interglacial (MIS 5e). Paleoceanography 27 PA2207.

Jimenez-Espejo, F.J., García-Alix, A., Jiménez Moreno, G., Rodrigo-Gámiz, M., Anderson, R.S., Rodríguez Tovar, F.J., Martínez Ruiz, F., Giralt, S., Delgado Huertas, A., Pardo Igúzquiza, E., 2014. Saharan aeolian input and effective humidity variations over western Europe during the Holocene from high altitude record. Chem. Geol. 374–375, 1–12.

Jochum, K.P., Nohl, U., Herwig, K., Lammel, E., Stoll, B., Hofmann, A.W., 2005. GeoReM: a new Geochemical database for reference materials and isotopic standards. Geostand. Geoanal. Res. 29, 333–338.

Kawahata, H., Okyrmoto, T., Matsumoto, E., Ujiie, H., 2000. Fluctuations of eolian flux and ocean productivity in the mid-latitude North Pacific during the last 200kyr. Quat. Sci. Rev. 9, 1279–1282.

Keigwin, L.D., 1998. Glacial-age hydrography of the far northwest Pacific Ocean. Paleoceanography 13, 323–339.

Khim, B.-K., Sakamoto, T., Harada, N., 2012. Reconstruction of surface water conditions in the central region of the Okhotsk Sea during the last 180 kyrs. Deep-Sea Res. II 61–64, 63–72.

Keigwin, L.D., Jones, G.A., Froelich, P.N., 1992. A 15,000 year paleoenvironmental record from Meiji seamount, far northwestern Pacific. Earth Planet. Sci. Lett. 111, 425–440.

Kimura, N., Wakatsuchi, M., 1999. Processes controlling the advance and retreat of sea ice in the Sea of Okhotsk. J. Geophys. Res. Oceans 104, 11137–11150.

Knudsen, K.-L., Seidenkrantz, M.-S., Kristensen, P., 2002. Last interglacial and early glacial circulation in the northern North Atlantic Ocean. Quat. Res. 58, 22–26.

Levitan, M.A., Lavrushin, Y.A., 2009. Sedimentation History in the Arctic Ocean and Subartic Seas. Lectures Notes in Earth Sciences. Springer

Levitan, M.A., Luksha, V.L., Tolmacheva, A.V., 2007. Sedimentation history in the northern Okhotsk Sea for the last 1.1 Ma. Lithology Mineral. Resources 227–246 (in Russian).

Lisiecki, L.E., Raymo, M.E., 2005. A Pliocene-Pleistocene stack of 57 globally distributed benthic $\delta^{18}O$ records. Paleoceanography 20 PA1003.

Liu, Y.-J., Song, S.-R., Lee, T.-Q., Lee, M.-Y., Chen, Y.-L., Chen, H.-F., 2006. Mineralogical and geochemical changes in the sediments of the Okhotsk Sea during deglacial periods in the past 500 kyrs. Global Planet. Change 53, 47–57.

Loutre, M.F., Berger, A., 2003. Marine Isotope Stage 11 as an analogue for the present interglacial. Glob. Planet. Change 36, 209–217.

Mackensen, A., Hubberton, H.W., Bickert, T., Fischer, G., Futterer, D.K., 1993. $\delta^{13}C$ in benthic foraminiferal tests of Fontbotia wuellerstorfi (Schwager) relative to $\delta^{13}C$ of dissolved inorganic carbon in Southern Ocean Deep Water: implications for glacial ocean circulation models. Paleoceanography 8, 587–610.

Mangini, A., Jung, M., Laukenmann, S., 2001. What do we learn from peaks of uranium

and of manganese in deep sea sediments? Mar. Geol. 177, 63–78.
Maslov, A.V., Krupenin, M.T., Ronkin, Y.L., et al., 2004. Fine alumosiliciclastic sediments of the strathotypic cross-section of the South Ural Middle Rhyphean: peculiarities of formation, composition and evolution of source provincies. Lithol. Miner. Resour. 4, 414–441 (in Russian).
Max, L., Lembke-Jene, L., Riethdorf, J.-R., Tiedemann, R., Nürnberg, D., Kühn, H., Mackensen, A., 2014. Pulses of enhanced North Pacific Intermediate Water ventilation from the Okhotsk Sea and Bering Sea during the last deglaciation. Clim. Past 10, 591–605.
Melles, M., Brigham-Grette, J., Minyuk, P.S., Nowaczyk, N.R., Wennrich, V., DeConto, R.M., Anderson, P.M., Andreev, A.A., Coletti, A., Cook, T.L., Haltia-Hovi, E., Kukkonen, M., Lozhkin, A.V., Rosén, P., Tarasov, P., Vogel, H., Wagner, B., 2012. 2.8 Million years of arctic climate change from lake El'gygytgyn, NE Russia. Science 337, 315–320.
Meyers, P.A., 1994. Preservation of elemental and isotopic source identification of sedimentary organic matter. Chem. Geol. 113, 289–302.
Meyers, P.A., 1997. Organic geochemical proxies of paleoceanographic, paleolimnologic, and paleoclimatic processes. Org. Geochem. 27, 213–250.
Meyers, P.A., Teranes, J.L., 2001. Sediment organic matter. In: Last, W.M., Smol, J.P. (Eds.), Tracking Environmental Changes Using Lake Sediments. Kluwer, Dordrecht, pp. 239–270.
Muhs, D.R., Simmons, K.R., Steinke, B., 2002. Timing and warmth of the Last Interglacial period: new U-series evidence from Hawaii and Bermuda and a new fossil compilation for North America. Quat. Sci. Rev. 21, 1355–1383.
Müller, P.J., Kirst, G., Ruhland, G., von Storch, I., Rosell-Melé, A., 1998. Calibration of the alkenone paleotemperature index $U_{37}^{K'}$ based on core-tops from the eastern South Atlantic and the global ocean (60°N-60°S). Geochem. Cosmochim. Acta 10, 1757–1772.
Nagashima, K., Tada, R., Tani, A., Toyoda, S., Sun, Y., Isozaki, Y., 2007. Contribution of aeolian dust in Japan Sea sediments estimated from ESR signal intensity and crystallinity of quartz. Geochem. Geophys. Geosyst. 8 Q02Q04.
Nakamura, K., Chang, Q., 2007. Precise determination of ultra-low (sub-ng g^{1}) level rare earth elements in ultramafic rocks by quadrupole ICP-MS. Geostand. Geoanal. Res. 31, 185–197.
Nimmergut, A., Abelmann, A., 2002. Spatial and seasonal changes of radiolarian standing stocks in the Sea of Okhotsk. Deep-Sea Res. I 49, 463–493.
Nürnberg, D., Tiedemann, R., 2004. Environmental change in the Sea of Okhotsk during the last 1.1 million years. Paleoceanography 19.
Nürnberg, D., Dethleff, D., Tiedemann, R., Kaiser, A., Gorbarenko, S.A., 2011. Okhotsk Sea ice coverage and Kamchatka glaciation over the last 350 ka -evidence from ice-rafted debris and planktonic $\delta^{18}O$. Palaeogeogr. Palaeoclimatol. Palaeoecol. 310, 191–205.
Ogi, M., Tachibana, Y., 2006. Influence of the annual Arctic Oscillation in the negative correlation between Okhotsk Sea ice and Amur River discharge. Geophys. Res. Lett. 33, L086709.
Okazaki, Y., Takahashi, K., Katsuki, K., Ono, A., Hori, J., Sakamoto, T., Uchida, M., Shibata, Y., Ikehara, M., Aoki, K., 2005. Late Quaternary paleoceanographic changes in the southwestern Okhotsk Sea: evidence from geochemical, radiolarian, and diatom records. Deep-Sea Res. Part II 52 (16–18), 2332–2350.
Okazaki, Y., Timmermann, A., Menviel, L., Harada, N., Abe-Ouchi, A., Chikamoto, M.O., Mouchet, A., Asahi, H., 2010. Deep water formation in the North Pacific during the last glacial termination. Science 329, 200–204.
Okazaki, Y., Kimoto, K., Asahi, H., Sato, M., Nakamura, Y., Harada, N., 2014. Glacial to deglacial ventilation and productivity changes in the southern Okhotsk Sea. Palaeogeogr. Palaeoclimatol. Palaeoecol. 395, 53–66.
Okunishi, T., Kishi, M.J., Ono, Y., Yamashita, T., 2007. A lower trophic ecosystem model including iron effects in the Okhotsk Sea. Cont. Shelf Res. 27, 2080–2098.
Oppo, D.W., McManus, J.F., Cullen, J.L., 2006. Evolution and demise of the Last Interglacial warmth in the subpolar North Atlantic. Quat. Sci. Rev. 25, 3268–3277.
Otosaka, S., Honda, M.C., Noriki, S., 2004. La/Yb and Th/Sc in settling particles: vertical and horizontal transport of lithogenic material in the western North Pacific. Geochem. J. 38, 515–525.
Otsuki, A.S., Watanabe, S., Tsunogai, S., 2003. Adsorption of atmospheric CO2 and its transport to the intermediate layer in the Okhotsk Sea. J. Oceanogr. 59, 709–717.
Otto-Bliesner, B.L., Marshall, S.J., Overpeck, J.T., Miller, G.H., Hu, A., 2006. CAPE last interglacial project members. Simulating arctic climate warmth and icefield retreat in the last interglaciation. Science 311, 1751–1753.
Parkinson, C.L., 2000. Variability of arctic sea ice: the view from space, an 18-year record. Arctic 53, 341–358.
Paytan, A., Kastner, M., Chavez, F., 1996. Glacial to interglacial fluctuations in productivity in the equatorial Pacific as indicated by marine barite. Science 274, 1355–1357.
Psheneva, O.Yu., Gorbarenko, S.A., 2013. Response of bottom environments in the central sea of Okhotsk to orbital- and millennial-scale climate changes during the last 130000 years according to benthic foraminifera. Doklady Earth Sci. II 1030–1033.
Rasmussen, S.O., Bigler, M., Blockley, S.P., Blunier, T., Buchardt, S.L., Clausen, H.B., Cvijanovic, I., Dahl-Jensen, D., Johnsen, S.J., Fischer, H., Gkinis, V., Guillevic, M., Hoek, W.Z., Lowe, J.J., Pedro, J.B., Popp, T., Seierstad, I.K., Steffensen, J.P., Svensson, A.M., Vallelonga, P., Vinther, B.M., Walker, M.J.C., Wheatley, J.J., Winstrup, M., 2014. A stratigraphic framework for abrupt climatic changes during the Last Glacial period based on three synchronized Greenland ice-core records: refining and extending the INTIMATE event stratigraphy. Quat. Sci. Rev. 106, 14–28.
Riethdorf, J.-R., Nürnberg, D., Max, L., Tiedemann, R., Gorbarenko, S.A., Malakhov, M.I., 2013. Millennial-scale variability of marine productivity and terrigenous matter supply in the western Bering Sea over the past 180 kyr. Clim. Past 9, 1345–1373.
Rogerson, M., Rohling, E.J., Weaver, P.P.E., Murray, J.W., 2004. The Azores Front since the Last Glacial Maximum. Earth Planet. Sci. Lett. 222, 779–789.
Rollinson, H., 1993. Using Geochemical Data: Evaluation, Presentation. Interpretation. Pearson Education Ltd., Edinburgh.
Saitoh, S., Kishino, M., Kiyofuji, H., Taguchi, S., Takahashi, M., 1996. Seasonal variability of phytoplankton pigment concentration in the Okhotsk Sea. J. Remote Sens. Soc. Jpn. 16, 86–92.
Sakamoto, T., Ikehara, M., Aoki, K., Iijima, K., Kimura, N., Nakatsuka, T., Wakatsuchi, M., 2005. Ice-rafted debris (IRD)-based sea-ice expansion events during the past 100 kyrs in the Okhotsk Sea. Deep-Sea Res. Part II 52, 2275–2301.
Sakamoto, T., Ikehara, M., Uchida, M., Aoki, K., Shibata, Y., Kanamatsu, T., Harada, N., Iijima, K., Katsuki, K., Asahi, H., Takahashi, K., Sakai, H., Kawahata, H., 2006. Millennial-scale variations of sea ice expansion in the southwestern part of the Okhotsk Sea during the past 120 kyr: age model and ice-rafted debris in IMAGES Core MD01-2412. Glob. Planet. Change 53, 58–77.
Salyuk, A., Sosnin,V., Obzhirov, A., Pavlova, G., Biebow, N., 2003. Water column studies. In: Biebow, N. et al. (Eds.), Cruise Reports: Leg 1 and Leg 2. GEOMAR Report 110, pp. 110–112.
Sato, M.M., Narita, H., Tsunogai, S., 2002. Barium increasing prior to opal during the last termination of glacial ages in the Okhotsk Sea sediments. J. Oceanogr. 58, 461–467.
Schouten, S., Hopmans, E.C., Schefub, E., Sinninghe Damsté, J.S., 2002. Distributional variations in marine crenarchaeotal membrane lipids: a new tool for reconstructing ancient sea water temperatures? Earth Planet. Sci. Lett. 204, 265–274.
Screen, J.A., Simmonds, I., 2010. The central role of diminishing sea ice in recent Arctic temperature amplicafication. Nature 464, 1334–1337.
Seki, O., Ikehara, M., Kawamura, K., Nakatsuka, T., Ohnishi, K., Wakatsuchi, M., Narita, H., Sakamoto, T., 2004. Reconstruction of paleoproductivity in the Sea of Okhotsk over the last 30 kyr. Paleocanography 19, 1016.
Seki, O., Nakatsuka, T., Kawamura, K., Saito, S., Wakatsuchi, M., 2007. Time-series sediment trap record of alkenones from the western Sea of Okhotsk. Mar. Chem. 104, 253–265.
Seki, O., Sakamoto, T., Sakai, S., Schouten, S., Hopmans, E.C., Sinninghe Damste, J.S., Pancost, R.D., 2009. Large changes in seasonal sea ice distribution and productivity in the Sea of Okhotsk during the deglaciations. Geochem. Geophys. Geosyst. 10, Q10007.
Seki, O., Bendle, J.A., Harada, N., Kobayashi, M., Sawada, K., Moossen, H., Inglis, G.N., Nagao, S., Sakamoto, T., 2014. Assessment and calibration of TEX_{86} paleothermometry in the Sea of Okhotsk and sub-polar North Pacific region: implications for paleoceanography. Prog. Oceanogr. 126, 254–266.
Shigemitsu, M., Narita, H., Watanabe, Y.W., Harada, N., Tsunogai, S., 2007. Ba, Si, U, Al, Sc, La, Th, C and 13C/12C in a sediment core in the Western Subarctic Pacific as proxies of past biological production. Mar. Chem. 106, 442–455.
Simizu, D., Ohshima, K.I., Ono, J., Fukamachi, Y., Mizuta, G., 2014. What drives the southward drift of sea ice in the Sea of Okhotsk? Prog. Oceanogr. 126, 33–43.
Sirocko, F., Seelos, K., Schaber, K., Rein, B., Dreher, F., Diehi, M., Lenne, R., Jager, K., Krbetscher, M., 2005. A last Eemian aridity pulse in central Europe during the last glacial inception. Nature 436, 833–836.
Sorokin, Y.I., Sorokin, P.Y., 1999. Production in the Sea of Okhotsk. J. Plankton Res. 21, 201–230.
Stirling, C.H., Esat, T.M., Lambeck, K., McCulloch, M.T., 1998. Timing and duration of the last Interglacial: evidence for a restricted interval of widespread coral reef growth. Earth Planet. Sci. Lett. 160, 745–762.
Sugisaki, S., Buylaert, J.P., Murray, A.S., Tsukamoto, S., Nogi, Y., Miura, H., Sakai, S., Iijima, K., Sakamoto, T., 2010. High resolution OSL dating back to MIS 5e in the central Sea of Okhotsk. Quat. Geochronol. 5, 293–298.
Suzuki, K., Hattori-Saito, A., Sekiguchi, Y., Nishioka, J., Shigemitsu, M., Isada, T., Liu, H., McKay, M.L., 2014. Spatial variability in iron nutritional status of large diatoms in the Sea of Okhotsk with special reference to the Amur River discharge. Biogeosciences 11, 2503–2517.
Takahashi, K., 1998. The Bering and Okhotsk Seas: modern and past paleoceanographic changes and Gateway impact. J. Asian Earth Sci. 16, 49–58.
Takahashi, K., Matsumoto, E., Watanabe, Y.W., 2000. The distribution of $\delta^{13}C$ in total dissolved inorganic carbon in the central North Pacific Ocean along 175°E and implications for anthropogenic CO_2 penetration. Mar. Chem. 69, 237–251.
Talley, L.D., 1991. An Okhotsk Sea water anomaly: implications for ventilation in the North Pacific. Deep-Sea Res. 38, 171–190.
Thomas, A.L., Henderson, G.M., Deschamps, P., Yokoyama, Y., Mason, A.J., Bard, E., Hamelin, B., Durand, N., Camoin, G., 2009. Penultimate deglacial sea-level timing from Uranium/Thorium dating of Tahitian corals. Science 324, 1186–1189.
Thompson, W.G., Goldstein, S.L., 2006. A radiometric calibration of the SPECMAP timescale. Quat. Sci. Rev. 25, 3207–3215.
Tsunogai, S., Ono, T., Watanabe, S., 1992. Increase in total carbonate in the western North Pacific water and a hypothesis on the missing sink of anthropogenic carbon. J. Oceanogr. 49, 305–315.
Wallace, J.M., 2000. North Atlantic Oscillantions/annular mode: two paradigms-one phenomenon. Q. J. R. Meteorolog. Soc. 126, 791–805.
Wang, K.-S., Shi, X.-F., Zou, J.-J., Kandasamy, S., Gong, X., Wu, Y.-H., Yan, Q.-S., 2017. Sediment provenance variations in the southern Okhotsk Sea over the last 180 ka: Evidence from light and heavy minerals. Palaeogeogr. Palaeoclimatol. Palaeoecol. 479, 61–70.
Wang, Y.J., Cheng, H., Edwards, R.L., An, Z.S., Wu, J.Y., Shen, C.-C., Dorale, J.A., 2001. A high-resolution absolute-dated Late Pleistocene monsoon record from Hulu cave, China. Science 294, 2345–2348.
Wang, Y., Cheng, H., Edwards, R.L., Kong, X., Shao, X., Chen, S., Wu, J., Jiang, X., Wang, X., An, Z., 2008. Millennial- and orbitalscale changes in the East Asian monsoon over the past 224,000 years. Nature 451, 1090–1093.
Weber, E.T., Owen, R.T., Dickens, G.R., Halliday, A.N., Jones, C.E., Rea, D.K., 1996.

Quantitative resolution of eolian continental crustal material and volcanic detritus in North Pacific surface sediment. Geochim. Cosmochim. Acta 62, 1735–1744.
Wong, C.S., Matear, R.J., Freeland, H.J., Whitney, F.A., Bychkov, A.S., 1998. WOCE Line P1W in the Sea of Okhotsk 2. CFCs and the formation rate of intermediate water. J. Geophys. Res. 103, 15625–15642.
Yamazaki, T., Inoue, S., Shimono, T., Sakamoto, T., Sakai, S., 2013. Sea-ice conditions in the Okhotsk Sea during the last 550 kyr deduced from environmental magnetism. Geochem. Geophys. Geosyst. 14, 5026–5040.
Yasuda, T., Asahara, Y., Ichikawa, R., Nakatsuka, T., Minami, H., Nagao, S., 2014. Distribution and transport processes of lithogenic material from the Amur River revealed by the Sr and Nd isotope ratios of sediments from the Sea of Okhotsk. Prog. Oceanogr. 126, 155–167.
Zahn, R., Winn, K., Sarnthein, M., 1986. Benthic foraminiferal $\delta^{13}C$ and accumulation rates of organic carbon: *Uvigerina peregrina* group and *Cibicidoides wuellerstorfi*. Paleoceanography 1, 27–42.
Ziegler, M., Lourens, L.J., Tuenter, E., Hilgen, F., Reichart, G.J., Weber, N., 2010. Precession phasing offset between Indian summer monsoon and Arabian Sea productivity linked to changes in Atlantic overturning circulation. Paleoceanography 25 PA3213.